

**ANALYSIS OF PARTICLE COMPOSITION, SIZE AND TEMPERATURE
BY FT-IR EMISSION/TRANSMISSION SPECTROSCOPY**Peter R. Solomon, Robert M. Carangelo, Philip E. Best,
James R. Markham and David G. Hamblen

Advanced Fuel Research, Inc., 87 Church Street, East Hartford, CT 06108

Many chemical and energy conversion processes involve multi-phase feed or product streams. Streams can consist of mixtures of solids, liquids and gases and in some cases, the important species may be in transition between phases (e.g. liquid fuel combustion which involves liquid fuel droplets, vaporized fuel and soot). Process monitoring requires the measurement of parameters for the separate phases. There are requirements for monitoring feedstocks and samples of the process stream as well as for in-situ monitoring. Fourier Transform Infrared (FT-IR) absorption spectroscopy has been used previously as an in-situ diagnostic for both gas species concentration and gas temperature determinations (1-9). This paper describes a new method being developed for on-line, in-situ monitoring of particle streams to determine their chemical composition, size, and temperature. The technique uses a FT-IR spectrometer to perform both emission and transmission (E/T) spectroscopy for a stream of particles. The technique has been applied to measure particle properties under a variety of circumstances and several examples are presented for measurements of temperature, composition and size.

The method was employed to address a controversy concerning coal optical properties recently raised by Brewster and Kunitomo (10). Their recent measurements suggest that previous determinations for coal of the imaginary part of the index of refraction, k , may be too high by an order of magnitude. If so, the calculated coal emissivity based on these values will also be too high. The E/T technique was employed to determine directly the spectral emittance, ϵ_{ν} , of coal and char particles as a function of coal rank, extent of pyrolysis and temperature. For one coal, the measured spectral emittance was compared with a calculated value obtained from the material's complex index of refraction $N = n + ik$, and particle size, using Mie theory. The complex index of refraction was determined using an extension of Brewster and Kunitomo's method for measuring k . The technique employs KBr and CsI pellet spectra and uses Mie theory and the Kramers-Kronig transforms to separate scattering and absorption effects. Good agreement has been obtained between the calculated and measured values of (ϵ_{ν}) confirming the contention that previously measured values of k are too high.

EXPERIMENTAL

Apparatus - The apparatus employed in the experiments consists of an FT-IR spectrometer coupled to a reactor, such that the FT-IR focus passes through the sample stream as shown in Fig. 1. Emission measurements are made with the movable mirrors in place. Transmission measurements are made with the movable mirror removed. The Fourier transform technique, in contrast to wavelength dispersive methods, processes all wavelengths of a spectrum simultaneously. For this reason it can be used to measure spectral properties of particulate flows, which are notoriously difficult to maintain at a constant rate. The emission and transmission can be measured for the same sample volume. The technique is extremely rapid; a low noise emission or transmission spectrum at low resolution (4 cm^{-1}) can be recorded in under a second. Also radiation passing through the interferometer is amplitude modulated, and only such radiation is detected. Because of its unmodulated nature, the particulate emission passing directly to the detector does not interfere with the measurements of scattering or transmission.

In an ideal emission-transmission experiment both measurements are made on the identical sample. In our case the emission and transmission measurements are made sequentially in time along the same optical path, for a sample flowing through the cell in a nominal steady condition.

Measurements - To determine the temperature, size or composition of particulate samples, measurements are made of the transmittance and of the radiance, from which we calculate a quantity which we call the normalized radiance. The normalized radiance is the radiance divided by (1-transmittance) (which in the absence of diffraction effects is a measure of intersected particle surface area for samples whose index of refraction is sufficiently different from the surrounding medium). This normalization allows the radiance from particles which fill only a fraction of the FT-IR aperture to be compared to a black-body standard obtained for the full aperture.

The transmittance, γ_{ν} , at wavenumber ν , is measured in the usual way

$$\gamma_{\nu} = I_{\nu} / I_{0\nu} \quad (1)$$

where $I_{0\nu}$ is the intensity transmitted through the cell in the absence of sample, while I_{ν} is that transmitted with the sample stream in place. The geometry for the transmittance measurement is illustrated in Fig. 2. With a particle in the focal volume, energy is taken out of the incident beam by absorption and scattering. The figure illustrates scattering by refraction of energy at the particles surfaces. Scattering will also be caused by reflection and diffraction. For particles $> 50 \mu\text{m}$ whose index of refraction is sufficiently different from the surrounding medium, almost all the energy incident on the particle is absorbed or scattered.

To measure the sample radiance, the power from the sample with background subtracted, S_{ν} , is measured, and converted to the sample radiance, R_{ν} , in the following way

$$R_{\nu} = S_{\nu} / W_{\nu} \quad (2)$$

where W_{ν} is the instrument response function measured using a cavity radiator. The radiance measurement detects both radiation emitted by the particle itself, as well as wall radiation scattered or refracted by the particle as illustrated in Fig. 2.

We calculate the normalized radiance (which we refer to as the E/T spectra), R^n , in the following way,

$$R^n = R_{\nu} / (1 - \gamma_{\nu}). \quad (3)$$

The complete analysis for the normalized emission will be presented elsewhere (11). For this discussion we consider the limit where particles are sufficiently large that they effectively block all the radiation incident on them, and their diffraction pattern falls completely within the angular acceptance aperture of the spectrometer. Then the normalized radiance has the simple form,

$$R^n = (1 - \epsilon_{\nu}) R_{\nu}^b(T_w) + \epsilon_{\nu} R_{\nu}^b(T_p) \quad (4)$$

where ϵ_{ν} is the spectral emittance and $R_{\nu}^b(T_w)$ and $R_{\nu}^b(T_p)$ are the theoretical black-body curves corresponding to the temperature of the wall (T_w) and particle (T_p), respectively. This equation will be used in the discussion of results to follow.

RESULTS

Temperature and Emisivity - To illustrate the measurements, we consider several simple cases. First we consider hot particles such as coal or char surrounded by cold

walls ($T_p \gg T_w$). Then according to Eq. 4,

$$R_{\nu}^n = \epsilon_{\nu} R_{\nu}^b(T_p). \quad (5)$$

If T_p is known, then ϵ_{ν} can be determined and vice-versa.

The first example is for char under conditions where the particles first reach equilibrium with a heated tube reactor (HTR) and then exit the reactor and pass the FT-IR aperture. The reactor has been described previously (12-14). The gas-particle mixture cools about 75°C between the reactor and the FT-IR focus as determined with a thermocouple (14). In Fig. 3 we show the radiance, (R_{ν}), 1- transmittance, ($1-\tau_{\nu}$), and the normalized radiance, (R_{ν}^n), from char emerging from the HTR at a temperature of 983 K. ($1-\tau_{\nu}$) is a measure of the intersected surface area of particles, i.e., 4% of the beam is blocked. The normalized radiance is compared with a number of grey body curves at different values of constant ϵ . The $\epsilon = 0.87$ curve at 1000 K gives best fit with the experimental data. The temperature is in good agreement with the thermocouple measurement.

The second example is for lignite particles at a temperature of 782 K, before any pyrolysis has occurred. The normalized radiance spectrum in Fig. 4a is compared to a grey-body ($\epsilon = .90$) at the average thermocouple temperature of 782 K. While the previously formed char shows a grey-body shape close to the average temperature, the lignite does not have a grey-body shape. The black-body and experimental curves are close only in the range 1600-1000 cm^{-1} where the emissivity, calculated from Eq. 5, (Fig 4b) is close to 0.9. These and other measurements (12-16) show that the particle's emissivity is size and temperature dependent. For the size of coal particles used here, only specific bands between 1600 cm^{-1} and 1000 cm^{-1} (corresponding to the strongest absorption bands in coal) have a spectral emittance near 0.9.

The result can be understood by considering that a particle's emittance is related to its absorbance. By Krichoff's law, particles will emit only where they have absorption bands. As discussed by Hottel and Sarofim (17), for large particles (where diffraction can be neglected) the absorption can be calculated from geometrical optics considering all possible rays through the particles. The absorption within the particle can be calculated using absorbance values measured by the KBr pellet method (15,18). Figure 4c shows the absorbance measured by the KBr pellet method. The correspondence between the high absorbance bands and the regions of high emissivity are apparent. The most significant difference between the spectra of Figs. 4a and 4c is the presence of a steeply sloping background going toward large wavenumbers in the pellet spectrum (Fig. 4c) and its absence in the emittance spectrum (Fig. 4b). The pellet spectrum is from a transmission measurement which does not distinguish between the absorption and scattered components of the total cross section. This problem is treated in the section on Calculated Emissivity.

The emittance varies with particle size as shown in Fig. 5. R_{ν}^n is smallest for small particle sizes and approaches the black-body curve for large size particles.

The spectral emittance varies with rank as shown in Fig. 6. The strongest feature is the emittance above 1700 wavenumbers which increases above 90% carbon. The increase in emittance above 90% carbon is consistent with a corresponding increase in the broad sloping absorbance observed in KBr pellet spectra for high carbon coals. This absorbance is believed to be due to electronic absorption of multi-ring aromatic hydrocarbons (19). The emittance of anthracite is close to grey body. The spectral emittance variation with rank is consistent with the functional group variation with rank.

Having demonstrated that the FT-IR method does give an appropriate temperature assuming $\epsilon \approx 0.9$ in the 1600 cm^{-1} to 1000 cm^{-1} region, the technique was used to determine particle temperatures for non-isothermal conditions in the HTR reactor (13,14). Figure 7 shows the E/T spectra for increasing time in the reactor. The FT-IR temperatures are in good agreement (within 25°C) with calculated temperatures and temperatures measured with a thermocouple (14).

We can also observe in Fig. 7, changes in emittance of particles as a function of the extent of pyrolysis. At 883 K all the bands present in coal can be seen, except that the hydroxyl peak is noticeably depleted. At 963 K a broad continuum, characteristic of char, is beginning to grow. By 1050 K we see almost a grey-body continuum with CO_2 and H_2O peaks superimposed. From the spectra discussed so far we can say that the spectral emittance of lignite of this size range increases continuously with pyrolysis, reaching a constant maximum of about 0.9 when pyrolysis is sensibly complete. The relationship of the development of the continuum char spectrum with the extent of pyrolysis will be the subject of a future investigation.

The other examples are from a reactor where the particles are surrounded by hot walls. For the case where the particles are at wall temperature, $T_p = T_w$, Eq. 4 reduces to

$$R_{\nu}^n = R_{\nu}^b(T_p) \quad (6)$$

Figure 8a displays R_{ν}^n in one such case. In this case we don't have to include particle emittance in the analysis, as it can be shown and Eq. 6 indicates, that any lack of emittance must be made up by scattered and reflected radiation. Indeed, the normalized emission is close in shape and amplitude to a black-body at the measured window height wall temperature (1225 K). The determination of T_p when T_p is of the same order of magnitude as T_w requires a knowledge of ϵ_{ν} at some wavenumber and use of the complete expression for R_{ν}^n (Eq. 4). Examples are discussed in reference (11).

Two additional examples are shown for the case $T_p \ll T_w$. Then Eq. 4 reduces to

$$R_{\nu}^n = (1 - \epsilon_{\nu}) R_{\nu}^b(T_w) \quad (7)$$

Figure 8b is for KCl, a non-absorbing particle and Fig. 8c is for coal which absorbs in specific bands. By Eq. 7, $R_{\nu}^n = R_{\nu}^b(T_w)$ for KCl, since $\epsilon = 0$. R_{ν}^n matches the black-body curve at the wall temperature of 1060 K. The E/T spectrum of the coal sample matches the wall black-body in regions where the coal is transparent (i.e., $\epsilon \approx 0$) but is lower where the coal has absorption bands. We can determine the emissivity $\epsilon = 1 - R_{\nu}^n/R_{\nu}^b(T_w)$ from these spectra. The emissivity for the lignite of Fig. 8c is shown in Fig. 8d. When compared to the emittance for the same coal at 782 K in Fig. 4b, the most significant difference is the larger hydroxyl band at low temperatures due to hydrogen bonding.

Composition - As illustrated in Fig. 2b, the normalized radiance, R_{ν}^n , is the wall radiance $R_{\nu}^b(T_w)$ attenuated over the chord d at the particle's absorbance bands. We can, therefore, use R_{ν}^n (e.g., Fig. 8c) to obtain the absorbance of the particle if we know the average chord length, d . This has been done using a ray optics model and a computed probability density function $P(d)$ for all possible chords d . A more detailed discussion will be presented elsewhere (20). Figure 9 shows a comparison between the absorbance spectra obtained for the same coal by three methods: a) a quantitative spectrum (i.e. for a known sample density) of a finely dispersed coal in a pressed KBr pellet; b) a non-quantitative photoacoustic spectrum for fine particles suspended on a thin membrane (21); and c) a quantitative E/T "absorbance" spectrum considered to

arise from the black-body furnace spectrum being attenuated by the particle over some effective sample thickness related to the shape and size of the particle. The details of the analysis to obtain the E/T absorbance spectra from the E/T spectra are discussed in (20).

The spectra have a number of similarities and differences. To compare the spectra, it should be noted that the KBr pellet absorbance spectrum is the sum of absorption plus a sloping background due mostly to scattering of radiation. The KBr pellet spectrum also has distortion of the bands (a dip at the high wavenumber side of the band and a sloping tail at the low wavenumber side of the band) due to the Christiansen effect (22). This effect is caused by variation in the real part of the index of refraction near the absorption band, which effects the scattering contribution. The photoacoustic spectrum is free of the scattering and Christiansen effects, but is non-quantitative and appears to be more sensitive to mineral components than to the organic components. On the other hand, the E/T absorbance spectra is free from scattering and band distortions and appears in reasonable quantitative agreement with the absorption component of the KBr pellet spectrum.

Size - Size information can be obtained from the $(1-\gamma)$ or R_{∞}^n spectra. Figure 5 shows the increase in the emissivity with particle size, especially in the region above 1700 wavenumbers. The average particle size can be determined from R_{∞}^n if the complex index of refraction of the material is known. Alternatively, $(1-\gamma)$ contains size information for particles with $D < 80 \mu\text{m}$. For example $(1-\gamma)$ in Fig. 3b increases at low wavenumbers (long wavelengths) due to diffraction effects. The shape may be calculated using Rayleigh theory for large particles (23) or Mie theory for small particles (24). While the effect is small for particles near $80 \mu\text{m}$ diameter, the diffraction effect increases as the particles decrease in size, and is very sensitive to size in the 1-30 μm range.

CALCULATED EMISSIVITY

The determination of spectral emittance is important for two reasons. The first is that knowledge of the spectral emittance is necessary for the measurement of particle temperatures. The second is that the spectral emittance or the emissivity (the average emittance over all wavelengths) must be known to calculate both the rate of particle heatup and the radiative energy released by the particle during gasification or combustion. For small particles, the spectral emittance is usually not measured. Rather, it is calculated using the complex index of refraction, $N = n + ik$, from the standard equations of electromagnetic theory. For spherical particles these calculations are performed using Mie theory.

Unfortunately, some controversy surrounds the value of k for coal. The problem was recently considered by Brewster and Kunitomo (10). Large variations in the value of k have been reported in the literature ranging from less than 0.1 to more than 0.5. Brewster and Kunitomo have suggested that a possible reason for these discrepancies is that previous measurements of k for coal using reflection measurements were highly inaccurate due to an inherent limitation in the ability to get sufficiently smooth, and homogeneous coal surfaces. Using a transmission technique for small particles in KBr, they obtained values of k which are more than an order of magnitude lower in most regions of the spectrum. If the previously measured values of k are too high, then values of emissivity based on them are also too high. Based on the values of emissivity presented above, this is indeed the case.

In this section, we compare the measured values of ϵ_p to predictions of Mie theory. For these calculations, the value of n and k were determined using KBr and CsI pellet spectra for coal, in an extension of the method of Brewster and Kunitomo (10). The results confirm the low values of k measured by Brewster and Kunitomo.

To determine $N = n + ik$ from pellet spectra we use Mie theory and the Kramers-Kronig transform. Mie theory is a general solution of Maxwell's equations for an isotropic, homogeneous sphere of index of refraction N_{ν} , imbedded in a medium of index of refraction \tilde{N}_{ν} (24). In general, the complex index of refraction contains all of the electromagnetic properties of the material, but the real and imaginary parts, n_{ν} , and k_{ν} , must be Kramers-Kronig transforms of each other (24). Physically, this relationship arises by requiring causality, i.e., the material cannot respond to radiation until after the incident radiation hits the material. In practice, we determine k_{ν} , perform a Fourier Transform into the time domain, force causality in the time domain, and then transform back to the frequency domain to obtain n (25). The complete description of the method will be the subject of a future publication, but briefly our procedure for determining n and k is as follows: 1) with trial values of $n = n_0$ (a constant) and $k = 0$ and a particle diameter D , for coal in KBr, we use Mie theory to calculate a smooth scattering curve. 2) This scattering curve, plus a constant to account for reflection from the pellet surface, is subtracted from the experimental spectrum and the result is assumed to be a pure absorption, A_{ν} , where

$$A_{\nu} = \frac{4\pi}{2.3026} \frac{k_{\nu}}{\lambda} \times \frac{\text{volume of coal}}{\text{area of pellet}} \quad (8)$$

3) Calculate k_{ν} from Eq. 8 and use the Kramers-Kronig transform to determine the correction to n . 4) Using these values of n , k , and D , Mie theory is used to predict a CsI pellet spectrum. Since the scattering above 4000 cm^{-1} depends largely on the product $(n_{\text{coal}} - n_{\text{medium}})D$, this 4th step allows us to determine D and n_0 . This procedure is repeated until we can predict both the KBr and CsI spectra with the same n , k and D . The results of this procedure are shown in Fig. 10. Figure 10a and 10b are the KBr and CsI pellet spectra for a Montana Rosebud coal. Values of $n_0 = 1.66$ and $D = 2.6$ microns were found to give reasonable fits to the data. Figure 10c shows the calculated n and k ; and Fig. 10d shows the absorbance due to k (which now depends only on the coal, not the pellet material). Figures 10a and 10b also show the calculated scattering contribution to the absorbance spectrum (which depends on the difference between the n for the coal and medium). The structure in the scattering curves is the Christiansen effect, and as can be seen from Figs. 10a and 10b, it is in the opposite direction for the KBr and CsI pellets. Figure 10d shows the calculated total spectrum for the CsI pellet which is the sum of the absorption and scattering comparison with the measured spectra (Fig. 10b). The agreement is quite good, most obviously for the Christiansen effect on the minimum near 1700 cm^{-1} .

For a particle radius of 25 microns, we use Mie theory with the n_{ν} and k_{ν} from Fig. 10c to predict the emittance spectrum of cold coal, Fig. 10e. This is compared to the measured emittance in Fig. 10f. The agreement is good.

ACKNOWLEDGEMENTS

The general E/T method development and measurements of temperature and emissivities were performed under DOE contract #DE-AC21-81FE05122, the measurement of composition and size under NSF SBIR Grant #CPE-8460379, the measurement of index of refraction and calculating of emissivities under DOE SBIR contract #DE-AC01-85ER80313. We wish to thank Woodrow Fiveland and Richard Wessel of Babcock and Wilcox for helpful discussions on the coal emissivity problems and John McClelland of Ames Laboratory for supplying the PAS spectrum.

REFERENCES

1. Liebman, S.A., Ahlstrom, D.H., and Griffiths, P.R., *Applied Spectroscopy*, **30**, #3, 355, (1976).
2. Erickson, M.D., Frazier, S.E., and Sparacino, C.M., *Fuel*, **60**, 263, (1981).
3. Solomon, P.R., Hamblen, D.G., Carangelo, R.M., and Krause, J.L., Coal Thermal Decomposition in an Entrained Flow Reactor; Experiment and Theory, 19th Symposium (International) on Combustion, 1139, The Combustion Institute, Pittsburgh, PA, (1982).
4. Solomon, P.R., Hamblen, D.G., and Carangelo, R.M., Applications of Fourier Transform Infrared Spectroscopy in Fuel Science, ACS Symposium Series, 205, 4, 77, (1982).
5. Ottensen, D.K. and Stephenson, D.A., *Combustion and Flame*, 46:95 (1982).
6. Ottensen, D.K. and Thorne, L.R., 1983 International Conference on Coal Science, Pittsburgh, PA, pg. 621, (Aug. 15-19, 1983).
7. Solomon, P.R., "Pyrolysis", in Chemistry of Coal Conversion, R.H. Schlosberg, Editor, Plenum Publishing, New York, NY, (1985) in press.
8. Solomon, P.R. and Hamblen, D.G., Measurements and Theory of Coal Pyrolysis, A Topical Report for U.S. Department of Energy, Office of Fossil Energy, Morgantown Energy Technology Center, Contract No. DE-AC21-81FE05122, (1984).
9. Solomon, P.R., Hamblen, D.G., and Carangelo, R.M., "Analytical Pyrolysis", K.J. Voorhees, (Editor), Butterworths London, Chapter 5, pg. 121, (1984).
10. Brewster, M.Q. and Kunitomo, T., *Trans. ASME*, **106**, 678, (1984).
11. Best, P.E., Carangelo, R.M., Markham, J.R., and Solomon, P.R., "FT-IR Emission - Absorption Measurements from Coal and Char: Temperature and Emittance", submitted to *Combustion and Flame*, (1985).
12. Solomon, P.R., Hamblen, D.G., Carangelo, R.M., Markham, J.R. and DiTaranto, M.B., ACS Div. of Fuel Chemistry Preprints, **29**, #2, 104, (1984).
13. Solomon, P.R., Serio, M.A., Carangelo, R.M., and Markham, J.R., ACS Division of Fuel Chemistry Preprints, **30**, #1, 266 (1985).
14. Solomon, P.R., Serio, M.A., Carangelo, R.M., and Markham, J.R., Very Rapid Coal Pyrolysis, Accepted for publication in *Fuel* (1985).
15. Solomon, P.R., Hamblen, D.G., Carangelo, R.M., Markham, J.R., and Chaffee, M.R., Application of FT-IR Spectroscopy to Study Hydrocarbon Reaction Chemistry, ACS Division of Fuel Chemistry Preprints, **30**, #1, 1, (1985).
16. Best, P.E., Carangelo, R.M. and Solomon, P.R., FT-IR Determination of Coal and Soot Particle Temperatures During Pyrolysis, ACS Div. of Fuel Chem. Preprints, **29**, #6, 249, (1984).
17. Hottel, H.C., and Sarofim, A.F., "Radiative Transfer", McGraw Hill Book Co., New York, (1967).
18. Solomon, P.R. and Carangelo, R.M., *Fuel*, **61**, 663, (1982).
19. van Krevelen, D.W., Coal, Elsevier Co., Amsterdam, (1961).
20. Solomon, P.R., Carangelo, R.M., Hamblen, D.G., and Best, P.E., "Infrared Analysis of Particulates by FT-IR Emission/Transmission Spectroscopy", submitted to *Applied Spectroscopy* for publication (1985).
21. This technique was developed by John McClelland of Ames Laboratory and the spectra were supplied by him.
22. Laufer, G., Huneke, J.T. Royce, B.S.H. Teng, Y.C., *Appl. Phys. Lett.*, **37**, 517, (1980).
23. Gumprecht, R.O. and Slipeivch, C.M., *J. Phys. Chem.*, **57**, 90, (1953).
24. Bohren, C.F. and Huffman, D.R., "Absorption and Scattering of Light by Small Particles," John Wiley and Sons, NY (1983).
25. Peterson, C.W. and Knight, B.W., *Journal of the Optical Society of America*, **63**, No. 10, pg. 1238 (1973).

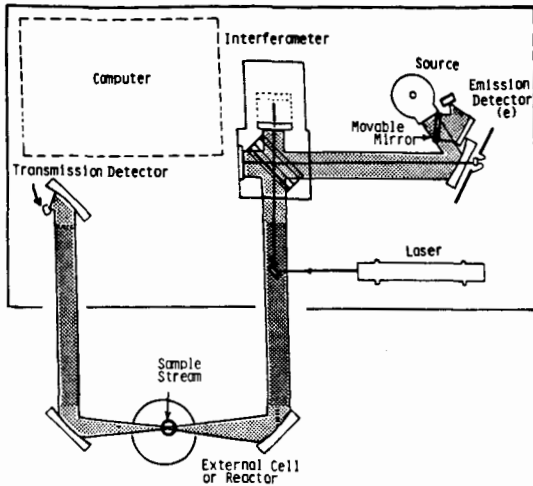


Figure 1. FT-IR Spectrometer with External Cell or Reactor.

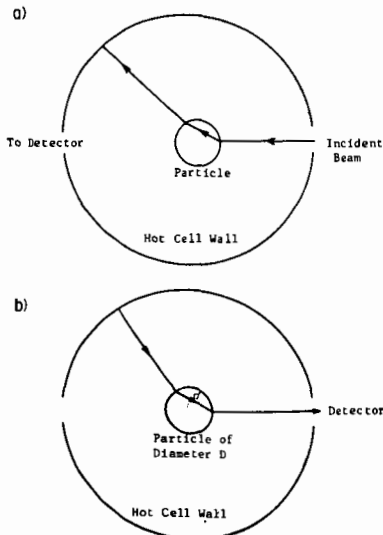


Figure 2. Measurement Geometry. a) Geometry of Transmission Measurement showing the Incident Beam Refracted by the Particle Out of the Beam; b) Geometry of Radiance Measurement showing Wall Radiance Refracted through a Particle to the Detector.

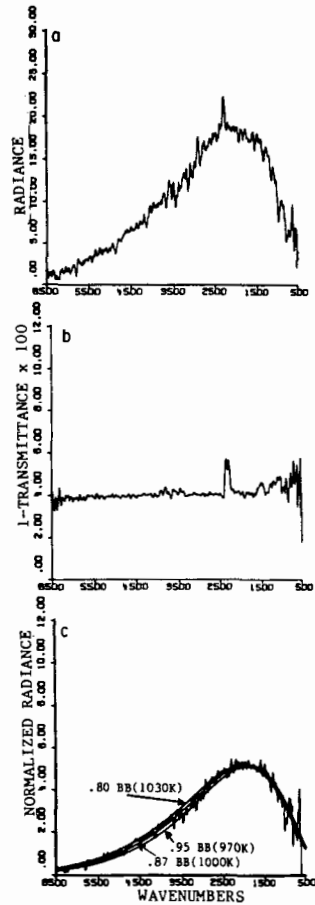


Figure 3. a) Radiance, b) (1-transmittance) and c) Normalized Radiance $R/(1-T)$ from Char Previously formed at 1300°C at an Asymptotic Tube Temperature of 1075 K , 115 cm Reaction Distance. In c) the Experimental Data is Overlaid by 3 Black-body Curves, the 1000 K being the Best Fit.

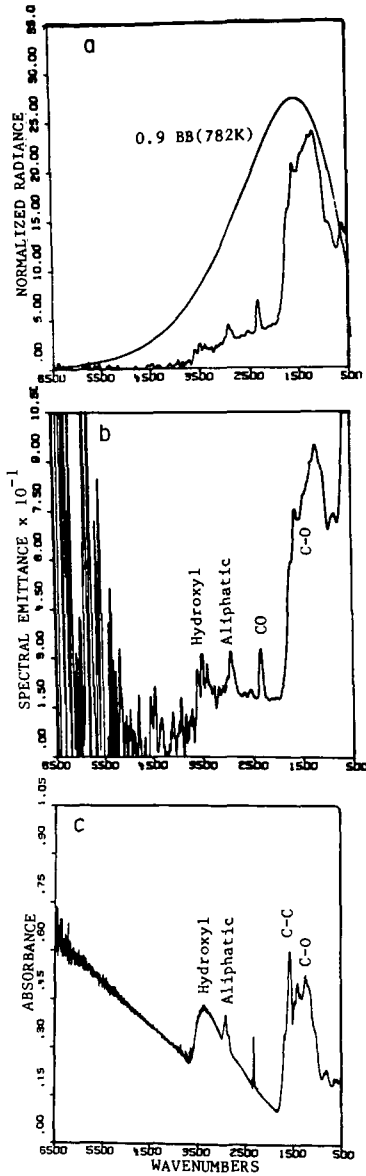


Figure 4. Spectra for Zap North Dakota Lignite a) Normalized Radiance, b) Spectral Emittance, and c) KBr Pellet Spectrum.

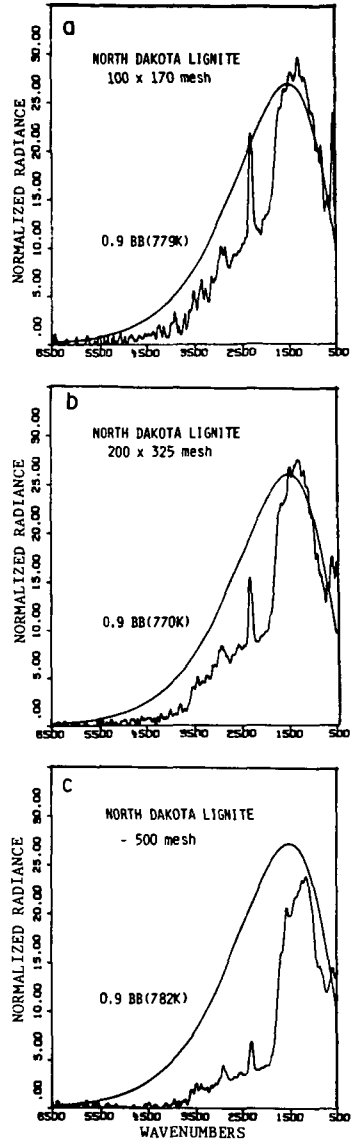


Figure 5. Normalized Radiance for Different Size Fractions of North Dakota Lignite.

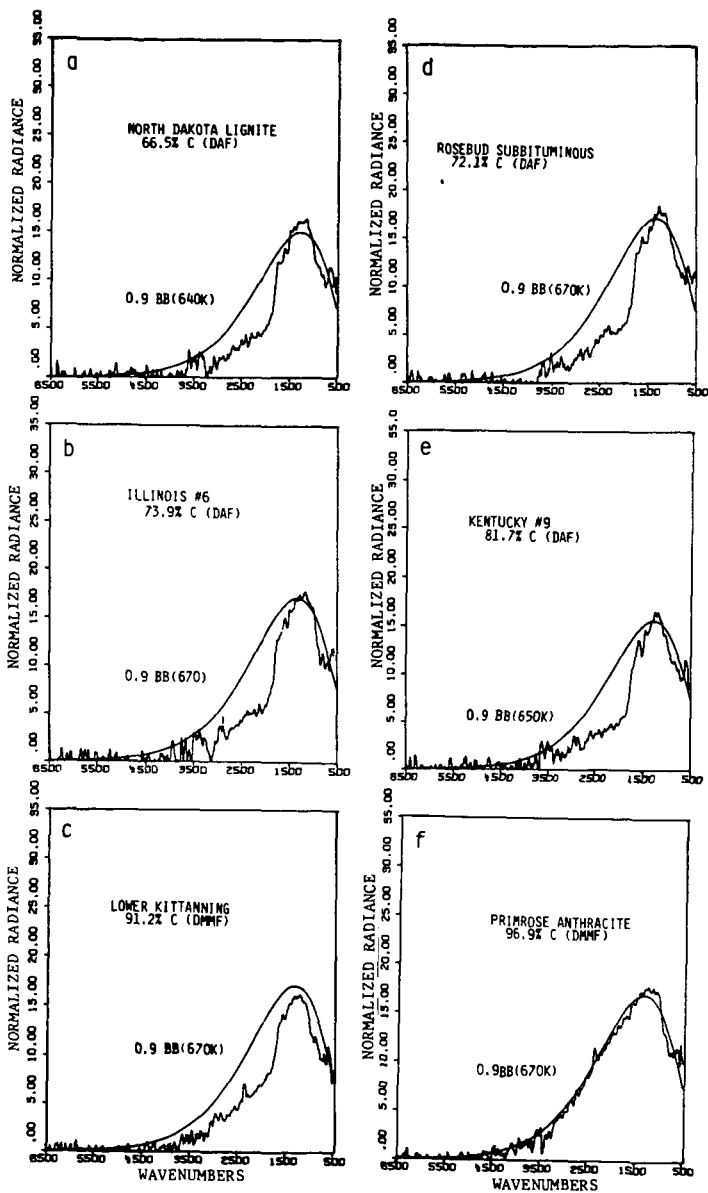


Figure 6. Comparison of Normalized Emission (Radiance) with Theoretical Grey-body Curves ($\epsilon = 0.9$) for Coals of Different Rank.

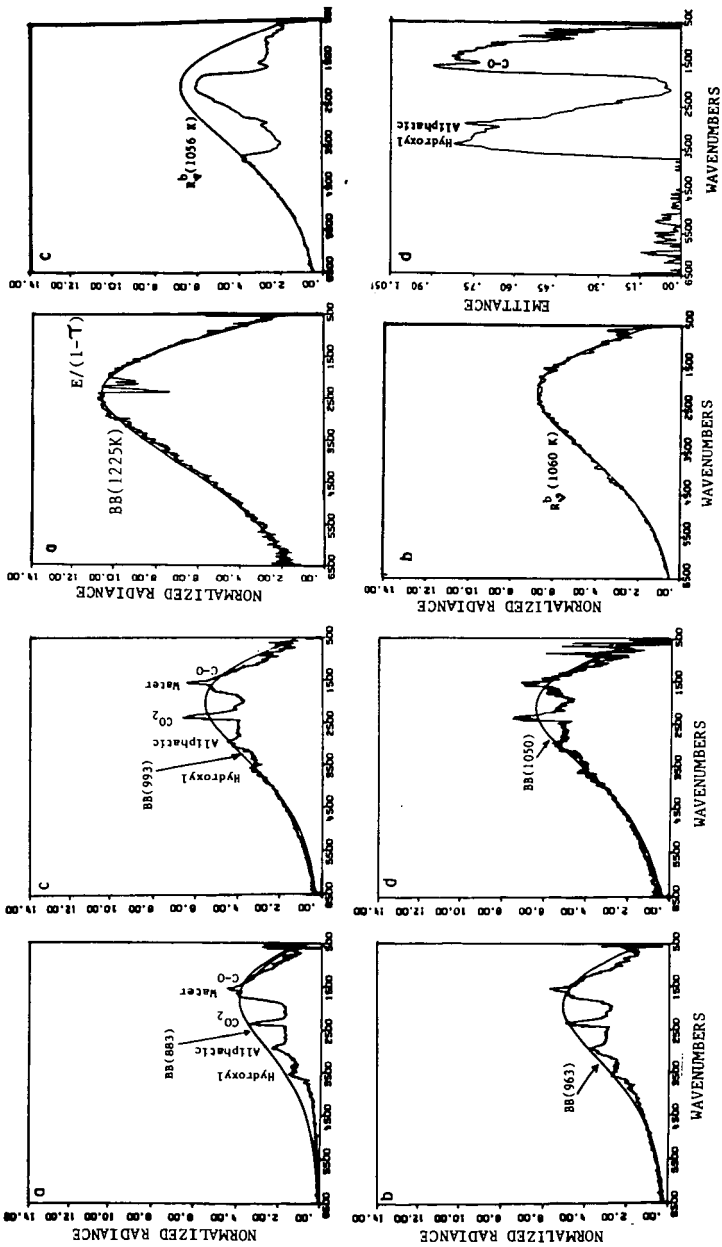


Figure 7. Comparison of Normalized Radiance with Theoretical Grey-Body Curves ($\epsilon = 0.9$) for Charts at Increasing Extents of Pyrolysis.

Figure 8. a-c) Comparison of Normalized Radiance with a Theoretical Black-body Curve for Several Cases. a) Coal, $T=1056$ K; b) KCl, $T=1060$ K; c) Coal, $T=1056$ K; d) Emissance derived from c) using Eq. 7.

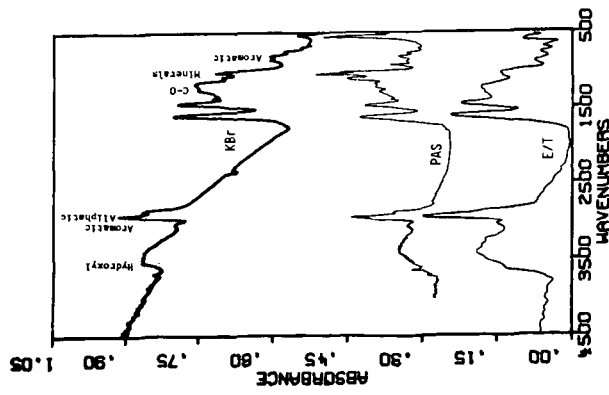


Figure 9. Comparison of Absorbance Spectra Obtained by KBr Pellet, Photoacoustic Spectroscopy (PAS), and E/T Methods. The KBr and E/T Spectra are Normalized to a 1 mg Sample in a 1.33 cm² area. The PAS Spectrum is Non-Quantitative.

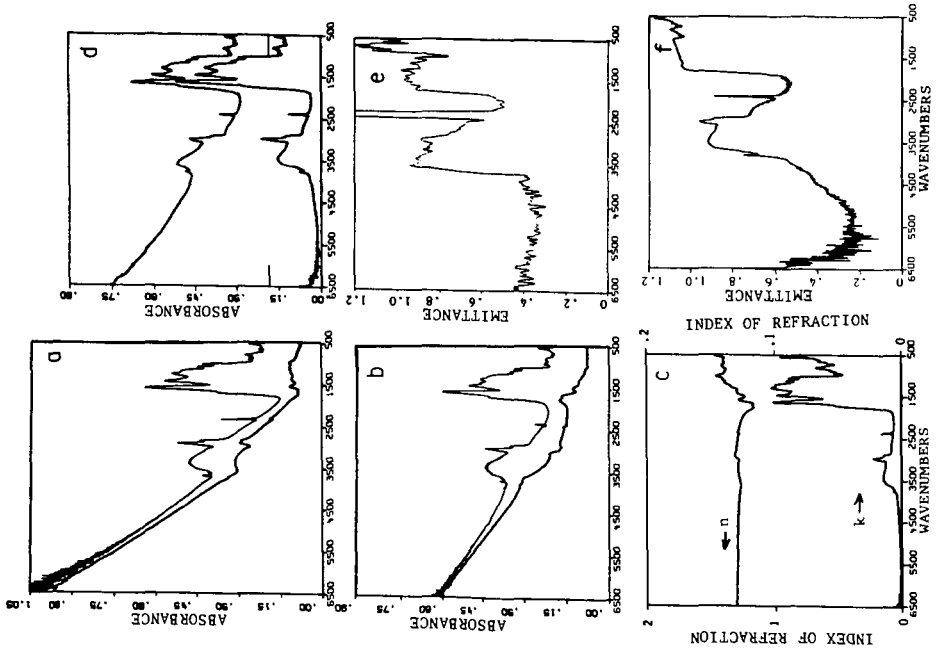


Figure 10. a) Measured Spectrum for Montana Rosebud in KBr with Part of Spectrum due to Scattering. b) Measured Spectrum for Montana Rosebud in Csi with Part of Spectrum due to Scattering. c) Real and Imaginary Parts of the Index of Refraction, $N = n + ik$. d) Upper Curve is Calculated Spectrum for Montana Rosebud in Csi, Lower Curve is Calculated Absorbance of Montana Rosebud without Scattering. e) Measured Emittance for Montana Rosebud, and f) Calculated Emittance for Montana Rosebud.